5th International Chemical Engineering Congress and Exhibition
Kish Island, 2 - 5 January 2008

Prediction of mixing time in a bubbly two-phase stirred tank by optical method

J. S. Moghaddas*, J. Revstedt[1], C. Trägårdh[2] and L. Fuchs[1]

* *Sahand University of Technology, P.O. Box 51335/1996, Tabriz, Iran*
[1,2] *Lund Institute of Technology at Lund University*
[1] *Division of Fluid Mechanics, P.O. Box 118, SE-221 00 Lund, Sweden*
[2] *Division of Food Engineering, P.O. Box 124, SE-221 00 Lund, Sweden*
* *Author to whom correspondence shall be addressed.*

Abstract

The mixing field in an aerated stirred reactor with two Rushton turbines was experimentally analysed using the particle image velocimetry and double-planer laser-induced fluorescence measurement techniques. The mixing characteristics were measured at three different impeller rotational speeds: 225, 300 and 400 rpm, for both single- and bubbly two-phase mixing systems. The mixing time was determined from the response curves to a pulse injection of a Rhodamine-590 tracer into the stirred tank. A considerable reduction in mixing time was achieved by increasing the impeller speed and implementing aeration.

Keywords: mixing, mixing time, two- phase flow, stirred tank, optical method, laser.

1. Introduction

Normally, in a mixing process in a stirred tank, any of the impellers centrally positioned produces rotating fluid motion with two vortices between each pair of blades, one above and one below the disk. The fluid in the vicinity of an eddy is highly sheared, resulting in the local reduction in a property, e.g. the concentration of a tracer. The swirling motion of the fluid causes a complex recirculating turbulent flow in the tank, where the stationary baffles interact with the flow improving the agitation. The fluid flowing away from the rotating impeller forms a jet towards the tank wall. After flowing vertically along the wall, the fluid will have a recirculation flow pattern towards the axis of the tank.

The circulation pattern of a fluid element in the vortices can be simply described as in Figure (1), which is adapted from Holmes et al. (1964). The circulation pattern for every fluid element above or below a turbine disk can be described in four stages: i) the jet flow running from the turbine towards the tank wall, ii) the vertical flow parallel to the tank wall, iii) the returning flow from the tank wall to the tank axis, and iv) the vertical flow along the tank axis towards the turbine.

In this study, the mixing time (q_{mix}) is defined as the time required to achieve 95% of the final concentration of the tracer in the stirred tank. Rielly and Britter (1985) studied mixing times experimentally by using the conductivity method. Assuming an idealised system in which there is no molecular diffusion of the tracer, they found that the impeller Reynolds number, $\mathrm{Re}_{imp} = \frac{N \cdot D^2}{u}$, of the flow affects the mixing. They also found that the tracer volume had no influence on mixing time. The mixing time may also be a function of the impeller speed, the geometry of the tank and impellers, the number of baffles and the physical properties of the fluids.

In the present work, using the particle image velocimetry (PIV) and double-planer laser-induced fluorescence (PLIF/PLIF) measurement techniques, the pumping

number and the mixing time were determined by studying the mean velocity of the liquid phase and the instantaneous concentration of a determining tracer. The influence of introducing bubbles as a dispersed phase on the mixing parameters was also investigated.

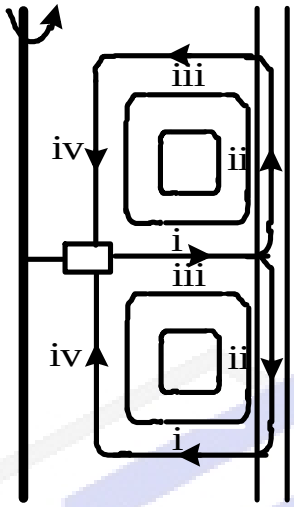

Figure 1. A schematic illustration of flow pattern with four stages for one side of an impeller inside the stirred tank.

2. Materials and Methods

The design and the dimensions of the stirred tank with two Rushton impellers of standard geometry, which were used in this work, are shown in Figure (2). The stirred tank consists of a flat-bottomed glass cylinder (refractive index 1.47 at a wavelength of 587 nm) an inner diameter T of 0.30 m. Four vertical baffles are symmetrically placed around the tank wall, each with a width of one-tenth of the tank diameter ($\ell_{baffle} = 0.1T$). The Rushton stirrer with two impellers, which is of standard design with a diameter (D) equal to one-third of the tank diameter ($D/T=1/3$), is located with a clearance from the tank bottom of about half of the tank diameter ($C_1=0.55T$). The upper impeller is placed $DC=0.7T$ above the lower one. A pump drives the turbines and the stirring speed is measured using a calibrated digital oscilloscope. In order to reduce optical refractive index effects at the cylindrical surface of the tank, it is placed in a square glass vessel. The stirred tank is filled with tap water as the main continuous phase fluid, the surface of which is $C_2=0.55T$ above the upper impeller. The square vessel is also filled with water to reduce light refraction at the interface. For more details on the geometry of the stirred tank used in this study see Guillard et al. (1999).

For the bubbly two-phase flow measurements, air bubbles are introduced, at a superficial gas velocity of 3.96×10^{-4} m/s 50 mm below the bottom impeller, through a sparger with a diameter of 3D/4 with 30 active orifices at the chosen gas flow rate.

A double-cavity 2×25 mJ Nd:Yag (Continuum) pulsed laser is used to produce a beam at a wavelength of 532 nm. The laser beam passes through a plano-concave lens to produce a two-dimensional vertical sheet of light (2 mm thick). Two series of experiments were performed: i) velocity measurements of the liquid phase using PIV,

and ii) concentration measurements of the determining tracer in the liquid phase using two CCD cameras (in PLIF/PLIF mode). In each series 3 different rotational speeds of the impellers: 225, 300 and 400 rpm, were employed. For the determination of the average velocity and mixing characteristics, each CCD camera captured 500 instantaneous images in each case. The average of the 500 images was used in the calibration of the PLIF/PLIF measurement. The calibration procedure is described by Moghaddas et al. (2002).

In the case of velocity measurements, the water in the tank was seeded with Rhodamine-B fluorescent tracer particles, 1-20 μm in diameter. The flow fields were measured at 23°, 30° and 37.5° angles behind the impeller blades for the three chosen rotational speeds of the impellers, i.e. 225, 300 and 400 rpm, respectively. A CCD camera with two long-pass filters, OG-550 and OG-570 (Melles Griot, Irvine, CA, USA) were used to capture the fluorescent signals from the particles. By masking the scattered signals from the bubbles using the two filters, only the signal from the seeding particles will be captured. The PIV image processing of the liquid continuous phase was performed using multipass interrogation windows decreasing from 32×32 to 16×16 pixels.

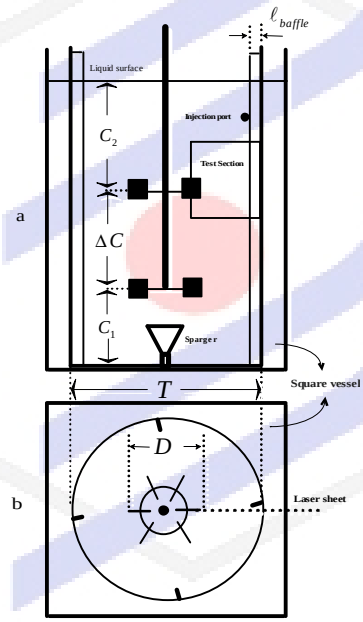

Figure 2. Stirred tank and impellers: a) side view, b) top view.

The concentration and mixing time measurements were carried out using the PLIF/PLIF technique. In this case the continuous phase was a well-mixed water solution of 131.5 μg/l of the reference tracer, LDS-722. Rhodamine-590 was selected as the determining tracer, as it has a high-emitted fluorescent intensity when irradiated with 563 nm light and a linear relation to concentration at low concentrations. To collect the laser-induced fluorescence of both the reference (LDS-722) and the determining (Rhodamine-590) tracers, two high-speed CCD cameras (La Vision, FlowMaster 3S) were used. The cameras were placed side by side on an aluminium plate. One CCD camera is used to record the fluorescence intensity of the reference tracer (LDS-722). This camera is equipped with two red optical filters, RG-665 and RG-695, with centre wavelength cut-offs of 665 and 695 nm, to ensure that only the

light emitted by this tracer is captured. The other CCD camera records fluorescence from the Rhodamine-590 tracer using two filters: one an OG-570 with a cut-off of 570 nm (centre wavelength), and the other an interference filter centred at 573 nm with $\Delta\lambda$=5 nm (Melles Griot, Irvine, CA, USA).

The Rhodamine-590 solution was injected through an injection port located below the liquid surface, on a baffle parallel to the sheet of laser light. The injection system consisted of a medical piston pump, which was easily controllable with regard to both injection speed and flow rate. A Rhodamine-590 tracer solution of 0.2 g/l with a constant flow rate 1.67 ml/s was injected during 1.5 seconds into the stirred tank. The change in the fluorescence signal from the tracer with time, at chosen pixel positions in the stirred tank, was then measured. Prior to each mixing time measurement, the fluorescence signal of the bulk solution, without the determining tracer, was measured to provide a background intensity. As the volume of each injected pulse is less than 1/550 000 of the fluid in the tank, it is assumed that the effect of the tracer on the flow pattern is negligible.

The mixing time, t_{95}, is defined as the time from the release of the determining tracer until the concentration of the tracer at a particular pixel reaches 95% of the final concentration in the tank. In practice, t_{95} is taken as the time, *t*, for the uniformity ratio of the concentration of the determining tracer, UR_c, to reach 0.05:

$$UR_c = \frac{C_\infty - C(i,j,t)}{C_\infty - C_0} \tag{1}$$

where C_0 and C_∞ are the initial tracer concentration and final or equilibrium concentration, respectively. The term $C(i,j,t)$ is the concentration at a point with location "*i*" in the radial direction and "*j*" in the axial direction, at some instant *t*, in time. The measured pixel mixing time, t_{95}, may differ slightly from one pixel to another, therefore the quantity UR_c is determined for all the pixels in the test section investigated and then the average mixing time is calculated using Eq. (2):

$$q_{mix} = \frac{1}{m}\sum_{i=1}^{m}\left[\frac{1}{n}\sum_{j=1}^{n} t_{95}(i,j)\right] \tag{2}$$

where *m* and *n* are the number of lines and columns of the concentration matrices in the measurements, respectively.

Assuming that the mixing process to be controlled by the rate of energy dissipation in the stirred tank, several empirical equations can be used to predict the mixing time. For example, Gao et al. (2003) proposed:

$$Nq_{mix} = 5.98 N_q^{-1/3} (T/D)^2 \tag{3}$$

where the coefficient of 5.98 is the experimental proportionality constant. Equation (3) shows that the product of the impeller speed and the mixing time, Nq_{mix}, would be proportional to $(T/D)^2$ based on the assumption that the impeller pumping capacity is independent of the D/T ratio.

3. Results and Discussion

Observation of the aerated bubbly two-phase flow pattern in the stirred shows that the bottom impeller disperses the bubbles coming from the sparger. Thus, most of the bubbles follow the downward liquid recirculation flow pattern before rising to the upper part of the tank. The bubbles from the recirculation stream together with some bubbles that are not captured by the downward fluid motion will then be transported above the bottom impeller. In this side the bubbles will pass the two recirculation vortices between the two impellers; the upward vortex of the bottom impeller and the downward vortex of the upper impeller. After passing the upper impeller the bubbles will follow almost a vertically rising flow in the upper part of the tank and will then break at the surface of the liquid. These observations are quite similar to the CFD results presented by Wu et al. (2000).

A typical average velocity field obtained from 500 instantaneous images at a chosen impeller rotational speed 300 rpm for the bubbly two-phase flow system is shown in Figure 3. Although the upper impeller stream region was of greater interest in this work, one can clearly recognise the upward and downward vortices of the impeller in this figure. The development of the jet flow field from behind the impeller blade towards the wall of the tank can also be seen. The jet-like pattern of the impeller stream decreases and the flow entrainment expands with increasing radial distance from the impeller.

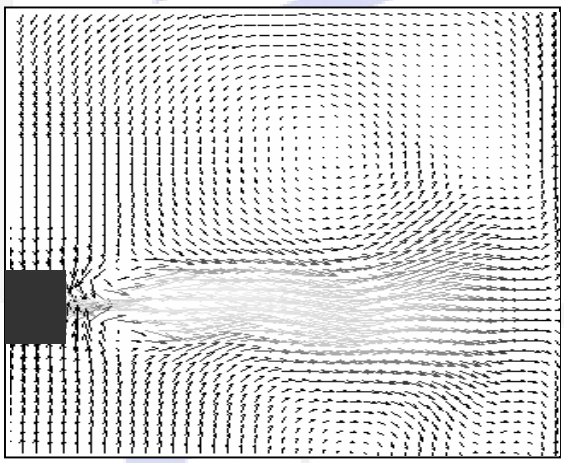

Figure 3. A typical mean radial continuous phase velocity image for bubbly two-phase flow at an impeller speed of 300 rpm.

Figure 4 shows the variation of the local radial velocity, U_r, as a function of the normalized axial distance and the normalized radial r/R positions, which is measured by Particle Image Velocimetery (PIV) technique. By examining the overall liquid velocity, it is clear that the mean velocity decreases from the impeller tip towards the tank wall. A comparison of the radial velocities in the impeller jet region reveals that the mean radial velocity decreases slightly when air bubbles are introduced.

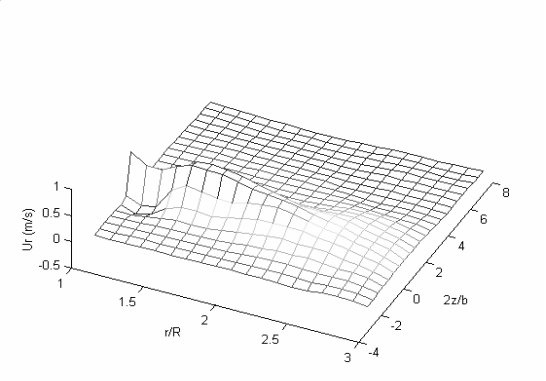

Figure 4. A typical mean radial velocity field of the liquid phase at an impeller speed of 300 rpm in bubbly two-phase flow.

Figure 5 shows the volumetric pumping flow rate for the region $1.52 \leq r/R \leq 2.16$ as a function of the dimensionless radius, impeller rotational speed and the aeration. As it noted earlier the tangential velocities can exceed the blade tip speed but according to Stoots and Calabrese (1995) in this region the normalized radial velocity is independent of the blade angle. Therefore, the PIV data for this region were used for the farther calculations. The figure shows that the volumetric discharge is directly proportional to the impeller speed and that it increases with radial distance from the impeller tip, due to fluid entrainment. However, it is only slightly reduced by introducing bubbles.

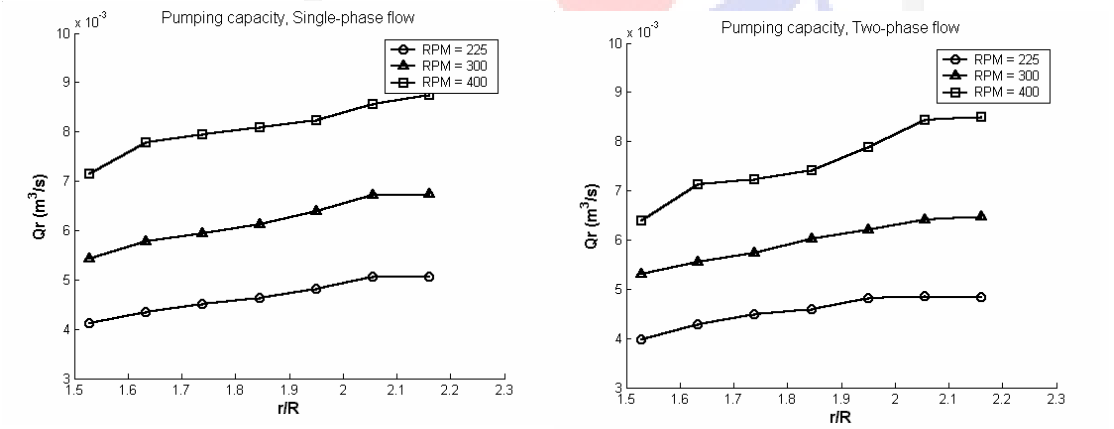

(a) (b)

Figure 5. Pumping flow rate for 3 different rotational speeds, 225, 300 and 400 rpm. a) Single-phase flow, b) two-phase flow.

Table 1 gives the calculated tip pumping numbers for all cases. In the case of single-phase flow it can be observed that the pumping number remains almost constant, with a mean value of 0.89, independent of the impeller rotational speed. These results are in very good agreement with the values obtained by Wu and Petterson (1989). The values of pumping number for the case of two-phase flow differ by the factor aerated-to-unaerated power ratio, which is the same effect as that on the normalised radial pumping flow rate.

At the aeration rate used the aerated stirring power in put (P_a) decreases with increasing impeller speed due to the decrease in the gas flow number (N_G), see Table 2. The relative power consumption was shown to be greater than 90% for all three impeller speeds without a strong drop, as was found by Bakker and van den Akker (1994b), in the range of $0.02 < N_G < 0.04$. Because in this study the values of gas flow numbers for every impeller speeds were less than the critical number of 0.02 found by them. A comparison between the theoretical and average experimental values of P_a/P_u shows quiet good agreement, spatially, for the two higher impeller speeds. Table 2 gives the calculated mixing characteristics of single- and bubbly two-phase flow for the three different rotational speeds.

Table 1. Calculated tip pumping numbers for 3 different rotational speeds, 225, 300 and 400 rpm.

RPM	**225**	**300**	**400**
Single-phase flow	0.89	0.87	0.92
Two-phase flow	0.90	0.86	0.72

Table 2. Calculated mixing characteristics of single- and two-phase flow for 3 different rotational speeds, 225, 300 and 400 rpm.

RPM	**225**	**300**	**400**
N (s^{-1})	3.75	5	6.67
U_{tip} (m/s)	1.18	1.57	2.09
Re_{imp}	3.75×10^{4}	5.00×10^{4}	6.67×10^{4}
N_G	7.66×10^{-3}	5.67×10^{-3}	4.25×10^{-3}
Pu (W/kg), (Eq. 3)	0.12	0.30	0.72
Pa/Pu (Eqs. 3 and 4)	0.90	0.93	0.95
Pa/Pu (Eq. 6)	0.97	0.96	0.93

Figure 6 shows a typical recording of the concentration of the Rhodamine-590 tracer as a function of time for a chosen pixel position, r/R = 1 and 2z/b = 2, above the impeller for a rotational speed of 225 rpm. As a highly concentrated tracer is injected above this position, in a short time a very high peak of fluorescent light will be observed at a pixel position in the region above the impeller. As the impeller redistributes the fluid element after every circulation loop more peaks will be recorded. In this study normally 2–4 peaks were observed at every point in this region, where the values and the number of peaks are a function of the impeller speed. For the positions in the impeller stream region, the concentration profiles, showing weaker peaks than those in the region above the impeller, will reach a final value. Below the impeller, the concentration profiles without early and high peaks monotonically increase to the final value.

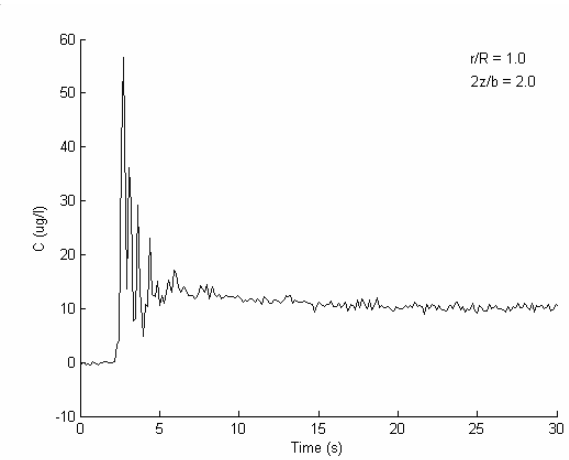

Figure 6. A typical measured profile of the concentration of the tracer as a function of time for a chosen pixel position, r/R = 1 and 2z/b = 2, at 225 rpm.

A pixel mixing time, t_{95}, for every point was measured by taking into account the 95% of the final concentration of the tracer by using Eq. (1). The global mixing time is then calculated using Eq. (2) by taking the averaged values of the mixing times at each pixel in the test section. Table 3 shows the measured global mixing time (s) for single- and two-phase flow at the three different rotational speeds. The results show that increasing the impeller rotational speed increases the liquid pumping capacity of the impeller and thus the mixing time decreases. Comparison the results for single- and bubbly two-phase systems show that introducing the bubbles improves the degree of liquid mixing by decreasing the mixing time for a particular impeller speed. Although the bubbles decrease the impeller pumping capacity, there could be an increase in the energy dissipation rate due to aeration according to Bakker and van den Akker (1994a).

Figure 7 shows a comparison between the maximum measured concentration of the tracer, in the test section region of each image, as a function of time an impeller speed of 300 rpm, for the single- and bubbly two-phase flow systems. In the bubbly two-phase flow system the scattering of the data is more pronounced than in single-phase flow.

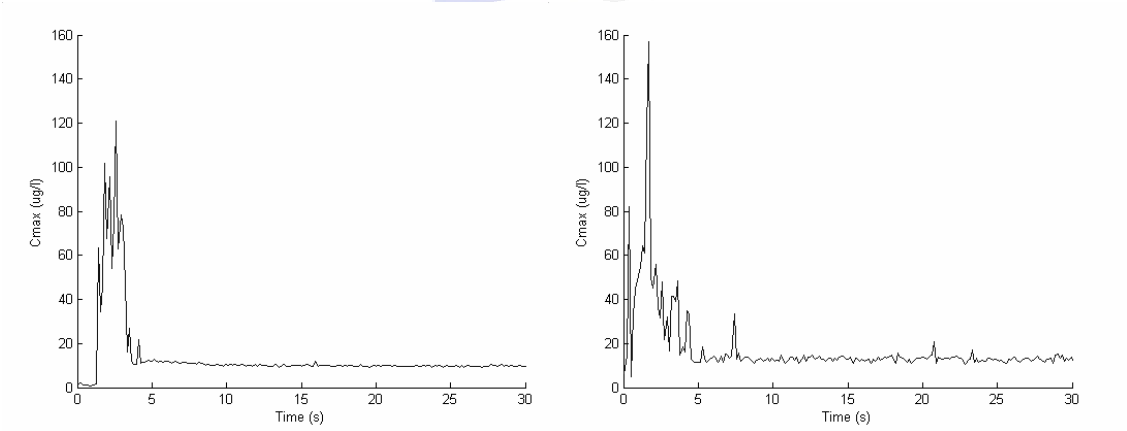

(a) (b)

Figure 7. Maximum concentration of the tracer as a function of time for 300 rpm. a) Single-phase flow, b) two-phase flow.

By comparing the results in Tables 2 and 3, one can also conclude that the mixing quality improves with increasing aerated power consumption in the bubbly two-phase system.

Based on Eq. (3) the following equations can be used to correlate the mixing time:

$$Nq_{mix} = A_u N_q^{u\,-1/3} (T/D)^2 \qquad \text{single - phase flow} \qquad (4)$$

$$Nq_{mix} = A_a (P_a / P_u)^{1/3} N_q^{a\,-1/3} (T/D)^2 \qquad \text{bubbly two - phase flow} \qquad (5)$$

where A is the experimental proportional coefficient and the indices *u* and *a* denote the unaerated and aerated flow systems, respectively. Average values of A_u = 5.43 and A_a = 4.87 were calculated by fitting the global mixing times at the three impeller speeds. The predicted value of A_u in this work is slightly less than that suggested by Gao et al. (2003), but it is in very good agreement with the value of 5.3 predicted by Ruszkowski (1994). Although in Eq. (5) the bubbly two-phase pumping number, N_q^a, is corrected by the aerated-to-unaerated power ratio, A_a is still less than A_u, which may be due to the increasing energy dissipation rate due to the bubbles.

Table 3. Measured global mixing time (s) for single- and two-phase flow at three different rotational speeds.

RPM	**225**	**300**	**400**
Single-phase flow	11.0	10.5	8.8
Two-phase flow	10.1	9.2	8.3

4. Conclusions

Using the particle image velocimetry (PIV) and double-planer laser-induced fluorescence (PLIF/PLIF) measurement techniques, the pumping number and the mixing time were determined by studying the mean velocity of the liquid phase and the instantaneous concentration of a determining tracer. The influence of introducing bubbles as a dispersed phase on the mixing parameters was also investigated. Visualisation of the dispersion of the bubbles near the upper impeller shows that the number density of the bubbles below the impeller is higher than above it. Bubbles coming towards the impeller from below will be dispersed by the impeller discharge. Depending on the relationship between the drag and the buoyancy of a bubble it will be transported to either the upper or lower recirculation vortex. Due to the small size of the bubbles in this study, they will probably mostly be transported to the lower part of the impeller discharge. Therefore, the volumetric void fraction of the bubbles is extremely unevenly distributed around the impeller. The mixing characteristics were measured at three different impeller rotational speeds: 225, 300 and 400 rpm, for both single- and bubbly two-phase mixing systems. Based on PIV results, the pumping capacity of the systems was calculated. The aerated-to-unaerated relative power was also calculated from the experimental results and compared with the theoretical values. The results show that the volumetric discharge is directly proportional to the

impeller speed and that it increases with radial distance from the impeller tip, due to fluid entrainment. However, it is only slightly reduced by introducing bubbles. Reasonable agreement between experimental and theoretical results was obtained. The mixing time was determined from the response to a pulse injection of a Rhodamine-590 tracer into the stirred tank. A considerable reduction in mixing time was achieved by increasing the impeller speed and implementing aeration.

Acknowledgements
The authors are grateful for the partial financial support of the Iranian Ministry of Science, Research and Technology and the Swedish Foundation for Strategic Research, programme for Multiphase Flow.

Notation

Q_p	impeller pumping capacity [m^3/s]
Q_r	radial pumping flow rate of the impeller [m^3/s]
D	impeller diameter [m]
b	blade height [m]
$\overline{U}_r$	average radial velocity at the blade tip over the height of blade [m/s]
N	impeller rotational speed [1/s]
N_q	pumping number [-]
N_q^a	pumping number for aerated system [-]
N_q^u	pumping number for unaerated system [-]
R	impeller radius [m]
r	radial location [m]
P_0	power number [-]
P_u	unaerated stirring power input [W/kg]
P_a	aerated stirring power input [W/kg]
NB_{imp}	number of impellers
V_{liq}	volume of liquid in the tank [m^3]
r	liquid density [kg/m^3]
N_G	gas flow number [-]
Q_g	gas flow rate [m^3/s]
q_{mix}	global mixing time [s]
t_{95}	pixel mixing time [s]
Re_{imp}	impeller Reynolds number [-]
u	kinematic viscosity of water [m^2/s]
ℓ_{baffle}	baffle width [m]
T	diameter of the tank [m]
C_0	initial tracer concentration [µg/l]
$C_¥$	final tracer concentration [µg/l]
$C(i,j)$	tracer concentration in pixel i , j [µg/l]
(i,j)	coordinate system based on camera geometry [-]
U_{tip}	impeller tip velocity [m/s]

References

Bakker A; van den Akker HEA (1994a) A computational model for the gas-liquid flow in stirred reactors. Trans IChemE 72: 594-606

Bakker A; van den Akker HEA (1994b) Gas-liquid contacting with axial flow impellers. Trans IChemE 72: 573-582

Gao Z; Niu G; Shi L; Smith J (2003) Mixing in stirred tanks with multiple hydrofoil impellers. Proceedings of 11th European conference on mixing: 557-564

Guillard F; Trägårdh C; Fuchs L (1999) A study of turbulent mixing in a turbine-agitated tank using a fluorescence technique. Experiments in Fluids 28: 225-235

Holmes DB; Voncken RM; Dekker JA (1964) Fluid flow in turbine-stirred, baffled tanks-I Circulation time. Chemical engineering Science 19: 201-208

Moghaddas J.S; Trägårdh C; Östergren K (2002) Use of a simultaneous PLIF-PLIF technique to overcome optical problems in concentration measurements in two-phase bubbly system. Advances in Fluid Mechanics IV, WIT_{PRESS}: 427-437

Rielly CD; Britter RE (1985) Mixing times for passive tracers in stirred tanks. 5th European conference on Mixing, Wurzburg, West Germany: 365-375

Ruszkowski S (1994) Proceedings of 8th European mixing conference, I. Chem. E., Rugby: 283-291.

Stoots CM; Calabrese RV (1995) Mean velocity field relative to a Rushton turbine blade. AIChE Journal 41: 1-11

Trägårdh Ch. (1988) A hydrodynamic model for the simulation of an aerated agitated fed-batch fermentor. Proceeding of the 2nd International Conference on Bioreactor Fluid Dynamics: 117-134

Vasconcelos JMT; Alves SS; Barata JM (1995) Mixing in gas-liquid contractors agitated by multiple turbines. Chemical Engineering Science 14: 2243-2354

Wu H; Patterson GK (1989) Laser-Doppler measurements of turbulent-flow parameters in a stirred mixer. Chemical Engineering Science 44: 2207-2221

Wu Z; Revstedt J and Fuchs L (2001) LES of a Two-Phase Turbulent Stirred Reactor. Turbulence and Shear Flow Phenomena 2, (Eds: Lindborg et al.), KTH Stockholm, vol. 2: 529-534